A Distributed Magnetostatic Resonator

Connor Devitt, *Graduate Student Member, IEEE*, Sudhanshu Tiwari, *Member, IEEE*, Sunil A. Bhave, *Senior Member, IEEE*, and Renyuan Wang, *Member, IEEE*

***Abstract*— This work reports the design, fabrication, and characterization of coupling-enhanced magnetostatic forward volume wave (MSFVW) resonators with significant spur suppression. The fabrication is based on surface micromachining of yttrium iron garnet (YIG) film on a gadolinium gallium garnet (GGG) substrate with thick gold transducers. A distributed resonator is used to excite forward volume waves in YIG to realize a frequency-dependent coupling boost. Fabricated devices at 18 and 7 GHz show coupling coefficients as high as 13% and quality factors above 1000. Higher order magnetostatic mode suppression is experimentally demonstrated through a combination of transducer and YIG geometry design.**

***Index Terms*— Magnetostatic wave (MSW), micromachining, tunable resonator, yttrium iron garnet (YIG).**

I. Introduction

NEXT-GENERATION RF front-end modules require low-loss and highly selective bandpass filters to cover the multitude of densely allocated frequency bands for commercial communication systems scaling beyond 6 GHz. Highly compact bandpass filters are also desired for wideband active electronically steered antenna arrays (AESAs), which are susceptible to interference and jamming when beamforming electronics are integrated at the element level. Including either tunable or arrays of selective filters between the antenna and receiver electronics mitigates this risk while maintaining the advantages of fully digital wideband AESAs [1], [2], [3]. Although significant progress has been made with a variety of electromagnetic filter technologies [4] in terms of synthesis, design, and manufacturing techniques, the filter size is fundamentally limited by the electromagnetic wavelength. Acoustic filters have seen significant commercial success for sub-6-GHz filtering due to their high quality factors (Q-factors), scalable fabrication, and compact size orders of magnitude smaller than their electromagnetic counterparts [5]. Scaling acoustic resonators toward higher frequency while maintaining high Q and large coupling coefficients to realize low loss, wide bandwidth filters remains an active area of research [6], [7], [8], [9], [10], [11].

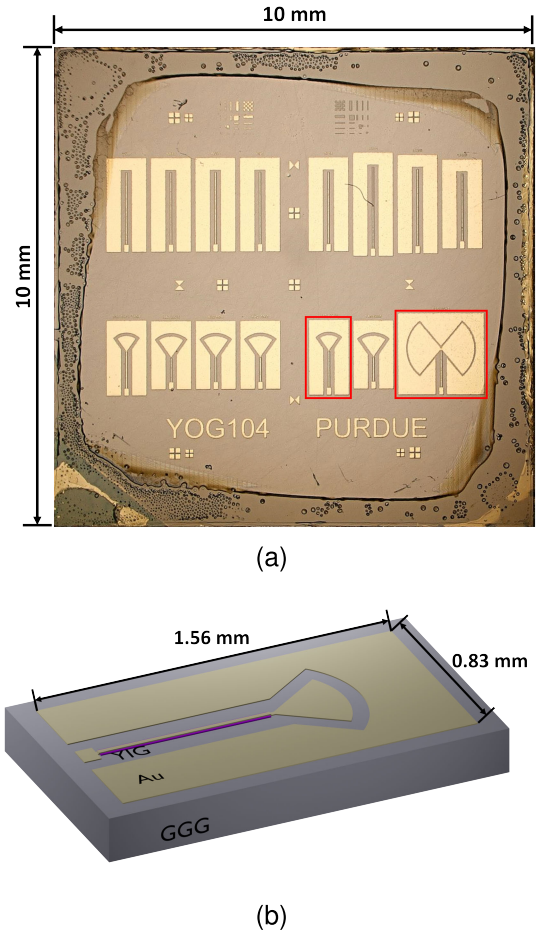

Fig. 1. (a) Microphotograph of multiple magnetostatic forward volume wave resonators fabricated on a YIG on GGG chip. Highlighted in red are two resonators designed at 18 GHz (left) and 7 GHz (right). (b) Rendering of the distributed resonator.

Filters based on magnetic materials such as yttrium iron garnet (YIG) have been an attractive technology for many years due to the material's magnetically tunable dispersion relationship and low Gilbert damping. The geometry of a magnetostatic wave (MSW) cavity can be designed independently of its bias-dependent resonant frequency allowing significant miniaturization over electromagnetic resonators. However, this technology has faced a number of integration and scaling challenges. Until recently, MSW filters were constructed out of flip-chip assemblies using bulk YIG and YIG on GGG

Manuscript received 27 January 2024; revised 12 March 2024; accepted 15 March 2024. This work was supported in part by the Air Force Research Laboratory (AFRL) and in part by the Defense Advanced Research Projects Agency (DARPA). *(Corresponding authors: Connor Devitt; Sunil A. Bhave.)*

Connor Devitt, Sudhanshu Tiwari, and Sunil A. Bhave are with the OxideMEMS Laboratory, Elmore Family School of Electrical and Computer Engineering, Purdue University, West Lafayette, IN 47907 USA (e-mail: devitt@purdue.edu; tiwari40@purdue.edu; bhave@purdue.edu).

Renyuan Wang is with the FAST Laboratory, BAE Systems, Inc., Nashua, NH 03060 USA (e-mail: renyuan.wang@baesystems.com).

Color versions of one or more figures in this article are available at https://doi.org/10.1109/TMTT.2024.3381549.

Digital Object Identifier 10.1109/TMTT.2024.3381549

chips [12], [13], [14], [15], [16], [17] or using polished YIG spheres manually aligned to 3-D transducers [18], [19], [20], [21]. Despite the high $Q > 3000$ [19] and low insertion loss below 2 dB [18] for YIG spheres and high $Q < 1600$ for YIG on GGG [22], this approached limits device size, fabrication scalability, and cost. The YIG needs to be biased with a strong magnetic field using either a rare-earth permanent magnet or a high-power electromagnet [18], [23], [24], increasing the system size and complexity despite the compact filter core. In addition, previously reported magnetostatic coupling coefficients of thin-film YIG (analogous to the acoustic piezoelectric effective coupling coefficient) have been small (<3%) [23], [25], [26] constraining the maximum filter bandwidth and limiting potential applications. Shorted microstrip transducers [27] can give relatively high coupling, but the resonator dimensions become moderately large. Recently, a low-power integrated tunable biasing method has been demonstrated in [23], allowing system miniaturization. Scalable lithographic fabrication methods have also been demonstrated using wet etching [23], [28], reactive ion etching (RIE) [29], and physical etching [25], [26], [30]. In this work, a new compact distributed resonator design is presented (Fig. 1) which enables wider bandwidth filters at the expense of magnetic tuning range.

II. Resonator Design and Modeling

In previous work, an MSW is excited in YIG using an inductive element with a frequency response modeled using the lumped circuit shown in Fig. 2(a) as reported in [25], [26], [30], [31], [32], and [33]. R_0 and L_0 represent the equivalent loss and inductance in the microwave transducer, respectively, while R_m, C_m, and L_m represent a single resonant MSW mode at a frequency f_m. The resonator exhibits an MSW resonance and anti-resonance for each excited mode whose frequency can be calculated from the YIG geometry using the dispersion relationship for the lowest order magnetostatic forward volume wave (MSFVW) [34]

$$\omega^2 = \omega_0\left[\omega_0 + \omega_m\left(1 - \frac{1 - e^{-k_{mn}t}}{k_{mn}t}\right)\right] \tag{1}$$

where $\omega_m = \mu_0\gamma_m M_s$, $\omega_0 = \mu_0\gamma_m H_{\text{dc}}^{\text{eff}}$, t is the film thickness, γ_m is the gyromagnetic ratio, μ_0 is the permeability of free space, k_{mn} is the wave vector, M_s is the saturation magnetization, and $H_{\text{dc}}^{\text{eff}}$ is the effective dc magnetic bias inside the film. The MSW is confined within the YIG mesa forming a number standing waves with discrete wave vectors k_{mn} related to the length and width of the YIG [15], [22], [25], [35]. Analogous to acoustic resonators, a magnetostatic effective coupling coefficient can be defined as [36]

$$k_{\text{eff}}^2 = \frac{\pi}{2}\left(\frac{f_1}{f_2}\right)\cot\left(\frac{\pi}{2}\frac{f_1}{f_2}\right). \tag{2}$$

For the shorted transducers [Fig. 2(a)], f_1 is the MSW resonance (f_m) and f_2 is the anti-resonance. With this model, k_{eff}^2 is a function of the ratio of L_m to L_0 and limits the maximum achievable filter bandwidth for a specified level of passband ripple. For acoustic resonators modeled using the Butterworth–Van Dyke circuit [37], k_{eff}^2 (related to the ratio of motional capacitance C_m to static capacitance C_0) also limits the maximum bandwidth. Several groups [38], [39], [40], [41], [42], [43], [44] have demonstrated micromechanical and bulk acoustic resonators with enhanced k_{eff}^2 beyond the material limited electromechanical coupling using inductors in parallel with the acoustic resonator to compensate for C_0. However, this approach incurs a significant cost to both filter area and insertion loss since the inductor's high resistive losses load the resonator's Q-factor. A similar approach can be used to enhance the magnetostatic coupling with a distinct advantage. For an MSW resonator, a series capacitor is required to compensate for L_0 which can be fabricated on chip with high Q-factors. Furthermore, the discrepancy between the electromagnetic and magnetostatic wavelengths is significantly smaller than that for an acoustic wave, allowing the MSW cavity's size to be on the order of the electromagnetic wavelength. As a result, an open-ended distributed element can introduce a compensating impedance with minimal cost to both area and Q-factor. This work demonstrates an order of magnitude increased effective coupling using a distributed electromagnetic resonator as the MSW transducer with only a 68% increase in resonator area at 18 GHz.

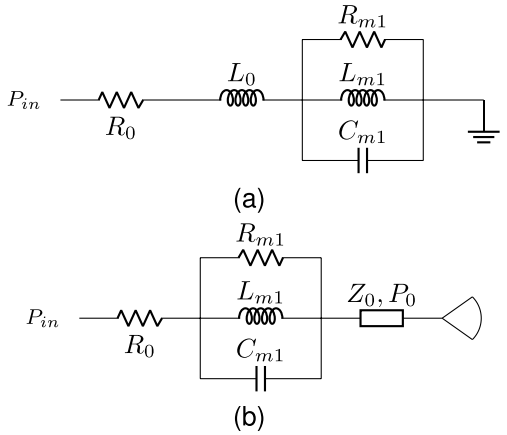

Fig. 2. (a) Conventional lumped element model for electrically short MSW resonators with shorted termination. (b) Distributed model for MSW resonators terminated with a high-frequency short where Z_0 and P_0 represent the characteristic impedance and physical length of a transmission line, respectively.

Fig. 1 shows a chip microphotograph of the fabricated coupling-enhanced MSFVW resonators, and Fig. 1(b) shows a rendering of one such resonator. Each resonator consists of a rectangular 3-μm-thick YIG mesa with length $\gg$ width and an open-ended 3-μm-thick conformal Au transducer over the YIG. At 0-Oe bias, the transducers are designed to provide a small resistive input impedance at either 7 or 18 GHz. For the top row of devices with 1500-μm-long Au and YIG, this is accomplished using a quarter-wave stub. The bottom row uses either 500-μm- or 750-μm-long YIG mesas terminated with a radial stub giving a low impedance, wide bandwidth short in a smaller form factor than the quarter-wave stub [45]. Near the electromagnetic resonance, f_{em}, the input impedance changes rapidly from capacitive to inductive and cannot be modeled using only the lumped inductor in

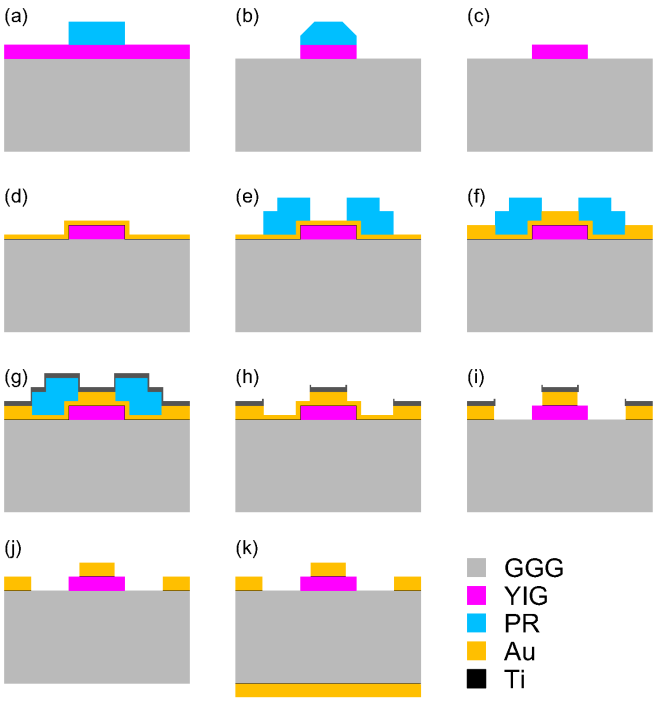

Fig. 3. Fabrication process of the MSW resonator: (a) 7.8-μm-thick photoresist (SPR220-7.0) is patterned as an etch mask on a 3-μm liquid phase epitaxy (LPE) YIG film grown on 500-μm GGG substrate. (b) 3-μm ion mill etch of the YIG film at a rate of 36 nm/min. (c) Photoresist mask is removed, and etched YIG is soaked in phosphoric acid at 80 °C for 20 min. (d) A blanket seed layer of 10-nm Ti and 300-nm Au is deposited using glancing angle e-beam evaporation. (e) A 10-μm-thick photoresist (AZ 10XT) mask is lithographically defined. (f) Patterned electroplating of 2.9 μm Au. (g) A 150-nm Ti etch mask is deposited using glancing angle e-beam evaporation. (h) Liftoff of Ti mask. (i) Au etch to remove blanket seed layer. (j) Ti etch. (k) Blanket 10-nm Ti and 300-nm Au are evaporated on the bottom of the substrate followed by electroplating of 3.0 μm of Au.

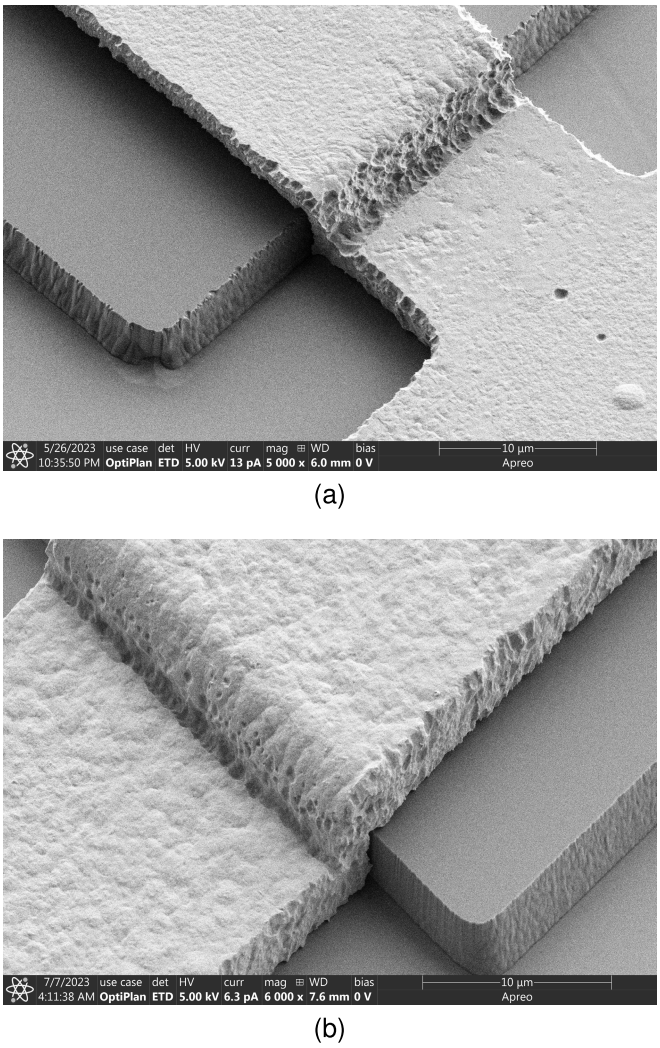

Fig. 4. Etched YIG and electroplated Au electrodes after final Au and Ti wet etches using (a) 70-nm e-beam evaporated Ti mask (not glancing angle) and (b) thicker 150-nm glancing angle e-beam evaporated Ti mask. In both the cases, the buffered oxide etchant undercuts the Ti adhesion layer beneath the electroplated Au.

Fig. 2(a). Instead, in Fig. 2(b), the inductor L_0 is replaced by a transmission line with impedance Z_0 and physical length P_0 (for both the quarter-wave stub and radial stub). The MSW resonance at f_m is approximately modeled using a parallel R-L-C configuration [46]. The interaction between the distributed resonator and the MSW will result in two anti-resonances: one below f_m and one above [38]. To account for both the anti-resonances as f_m is tuned, the coupling coefficient (2) is modified as follows: $f_2 = f_m$ if $f_m < f_{\text{em}}$ and otherwise $f_1 = f_m$. The coupling reaches a maximum when $f_m = f_{\text{em}}$.

III. Fabrication

The fabrication process for the MSFVW resonators is outlined in Fig. 3. The YIG etching in steps (a)–(c) is adapted from and described in detail in [30], [26], and [25]. Starting with a 3-μm YIG film epitaxially grown on a 500-μm-thick GGG substrate, the YIG mesas are patterned through ion milling using a thick photoresist (PR) mask. After ion milling, the sample is cleaned and soaked in hot phosphoric acid to remove the re-sputtered material. At this point, the MSW resonator is defined, but the microwave transducers must still be deposited. Based on [25], 300-nm-thick Au transducers showed significant conductor losses so the process presented here is optimized for thick Au transducers. A patterned electroplating process [47] is developed as a cost-effective alternative to evaporation and liftoff [48]. A 10-nm Ti adhesion layer and blanket 300-nm Au seed layer are first evaporated at a glancing angle to ensure coverage on the sidewalls of the etched YIG. The transducer geometry is lithographically defined using 10-μm-thick AZ-10XT PR chosen for compatibility with the electroplating solution. Using the blanket seed layer as an electrode, 2.9-μm Au is electroplated around the PR pattern. To protect the thick Au transducers during the seed layer removal, a Ti wet etch mask is evaporated and patterned by liftoff of the PR mask. The sample is submerged in Au enchant to remove the seed layer followed by buffered oxide etchant (BOE) to remove the Ti adhesion layer and etch mask. Initially, the Ti mask was 70-nm thick and evaporated at normal incidence yielding the transducer in Fig. 4(a) after the Au/Ti wet etches. The top surface of the plated Au shows randomly distributed pitting indicating pin holes in the mask and the etchant attacked the Au on the edge of the YIG mesa since the evaporated Ti

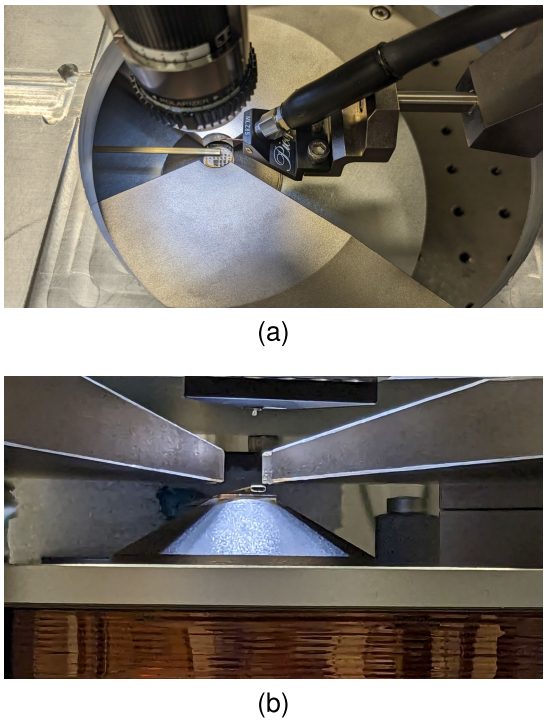

Fig. 5. Photographs of the measurement setup for the fabricated 10 × 10 mm resonator chip. (a) Top-down view of the setup showing the optical microscope, a nonmagnetic GSG probe, and a Gauss meter in close proximity to the chip resting on the electromagnet. (b) Side view of the setup with the chip resting flat on the pole of the electromagnet.

mask was not conformal. In the next device iteration, a thicker 150-nm Ti mask was used to minimize any pin holes and glancing angle e-beam evaporation was used to ensure conformal Ti coverage over the edge of the YIG mesa. In addition, the Ti adhesion layer beneath the electroplated Au is undercut by the BOE. Finally, 10-nm Ti and 300-nm Au are evaporated followed by 3-μm Au electroplating on the back side of the chip.

IV. Resonator Measurement

The one-port s-parameters are measured using an Agilent PNA E8364B with nonmagnetic GSG probes at an input power of −15 dBm. The out-of-plane magnetic field is generated using a constant current source and a single-pole electromagnet with a 10-mm pole face diameter. A single-axis Gauss meter attached to a probe manipulator is positioned closely above the sample near the device under test (DUT) to estimate the magnitude of the applied field. To ensure a uniform bias field across the entire length of the YIG mesa, the DUT is aligned to the center of the pole face using an optical microscope and secured in place using an adhesive. Fig. 5 illustrates the measurement setup for the MSW resonators.

Fig. 6(a) shows the frequency response of the 18-GHz resonator (highlighted in Fig. 1) terminated with a radial stub biased at 7714 Oe along with the simulated distributed circuit model using the fit parameters listed in Fig. 6(c). The distributed model shows good agreement with the measured frequency response and accurately captures the frequency dependence of the coupling as shown in Fig. 6(b) by sweeping

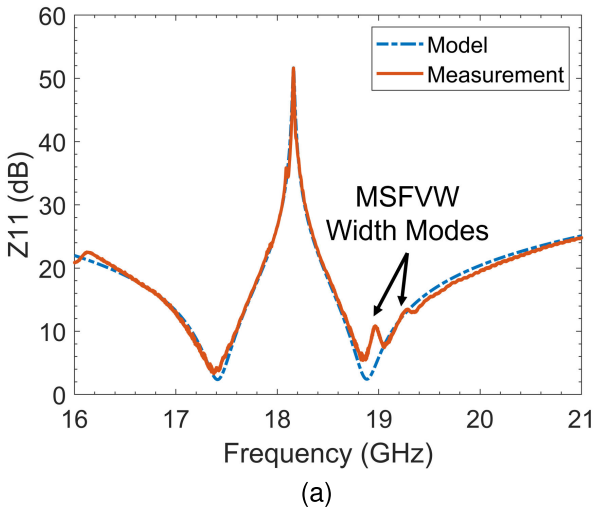

(a)

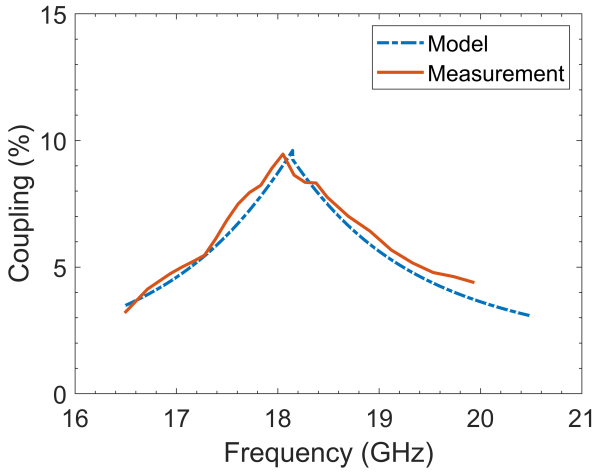

(b)

Model Parameters						
R_0	Z_0	P_0	R_m	L_m	f_m	ε_r
1.256 Ω	75.51 Ω	1622 µm	381.7 Ω	3.414 pH	18.16 GHz	6.5

(c)

Fig. 6. (a) Measured resonator impedance response biased at 7714 Oe showing a Q-factor of 1274 and simulated response from the fit distributed circuit model. (b) Measured resonator coupling from 7163 to 8310 Oe and simulated model coupling sweeping f_m from 16.5 to 20.5 GHz. (c) Fit distributed circuit model parameters at a 7714-Oe bias.

f_m. A Smith plot of the resonator response is provided in the Appendix. Figs. 7 and 8 show the measured frequency response, quality factors, and coupling factors of the two characteristic devices highlighted in Fig. 1 designed at 18 and 7 GHz. In both, the YIG mesa is 40-μm wide and 750-μm long while the Au transducer is 20-μm wide. Only the designed frequency of the radial stub differs between the two. Finite element simulations using Ansys HFSS revealed that increasing the width of the Au transducers relative to the YIG width helped suppress higher order MSFVW width modes, so two sets of resonators were fabricated. The first with YIG dimensions of 40 μm by 1500 μm and gradually increasing transducer widths from 6 to 25 μm and the second

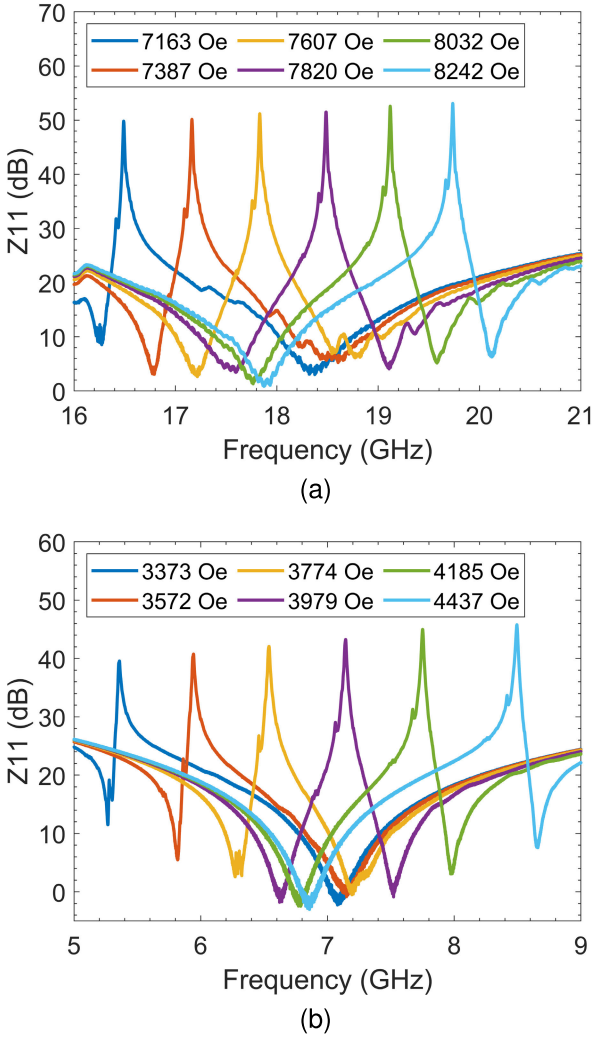

Fig. 7. Measured impedance over bias field for (a) 18-GHz and (b) 7-GHz resonators.

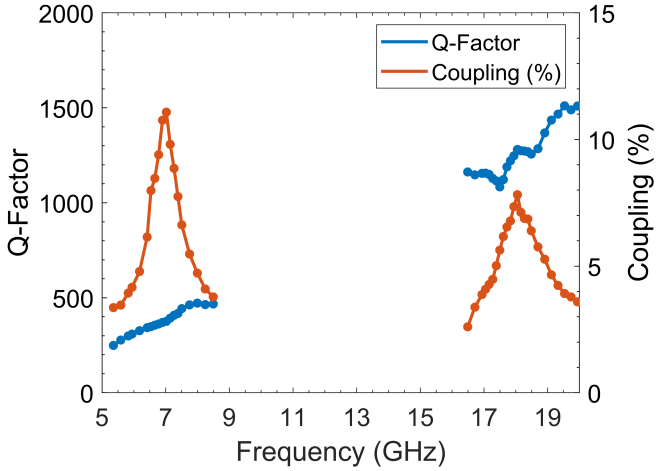

Fig. 8. Extracted Q-factor and coupling over bias field for two distinct resonators designed at 7 and 18 GHz.

with a constant 15-μm transducer width and a YIG length of 1500 μm with gradually increasing YIG widths from 40 to 60 μm. The relative spur levels defined as the impedance

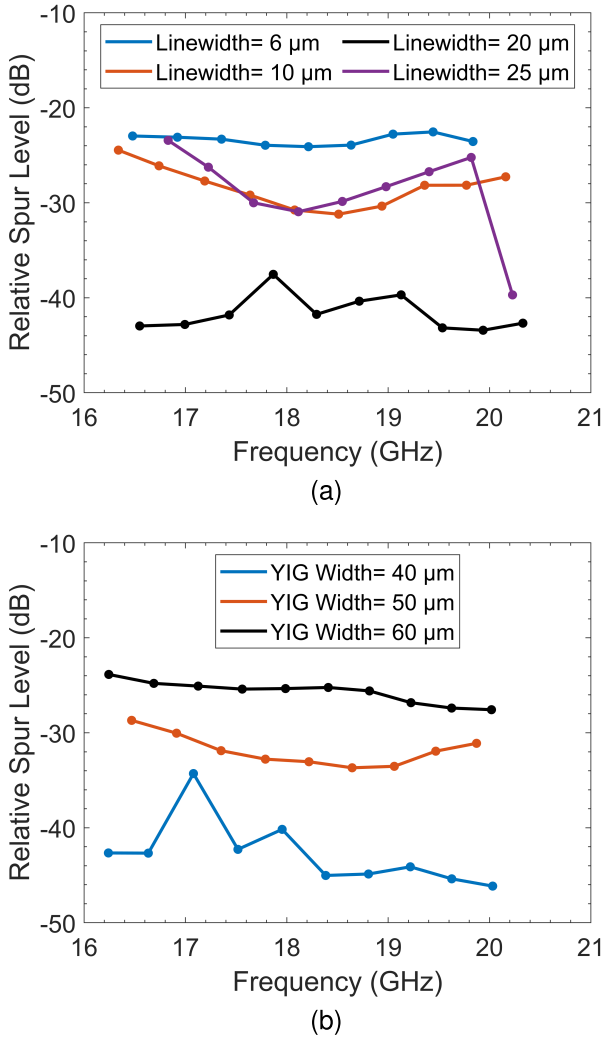

Fig. 9. Measured impedance of width-mode spur level relative to the main resonance over resonant frequency. (a) YIG resonator width is fixed to 40 μm and the linewidth of the gold transducer is varied. (b) Gold transducer width is fixed to 15 μm and the YIG resonator width is varied.

difference (in dB) between the main resonance and the first MSFVW width mode are summarized in Fig. 9. Based on these results, optimal spur suppression is achieved when the ratio of transducer width to YIG width is between 0.375 and 0.5. For the 40-μm-wide YIG resonator, the transducer shows a split resonance (at 0 Oe) which artificially enhances the impedance level of the spurious width mode when the resonator is biased at 17.1 GHz. Fig. 10 summarizes the trends in the Q-factor over YIG width and transducer width. Fig. 10(a) shows no clear trend in Q-factor over transducer width. Fig. 10(b) indicates that a wider YIG mesa can substantially improve Q-factor. The 60-μm-wide YIG resonator shows peak broadening in the impedance spectrum resulting in degraded Q-factor between 17.6 and 18.8 GHz. The broadening is attributed to an inhomogeneous magnetic bias along the length of the YIG. Above 18.8 GHz, the inhomogeneity is not observed and the Q-factor increases. The resonator coupling factor exhibited an increasing trend as the YIG mesa width decreased. The coupling also shows an increasing

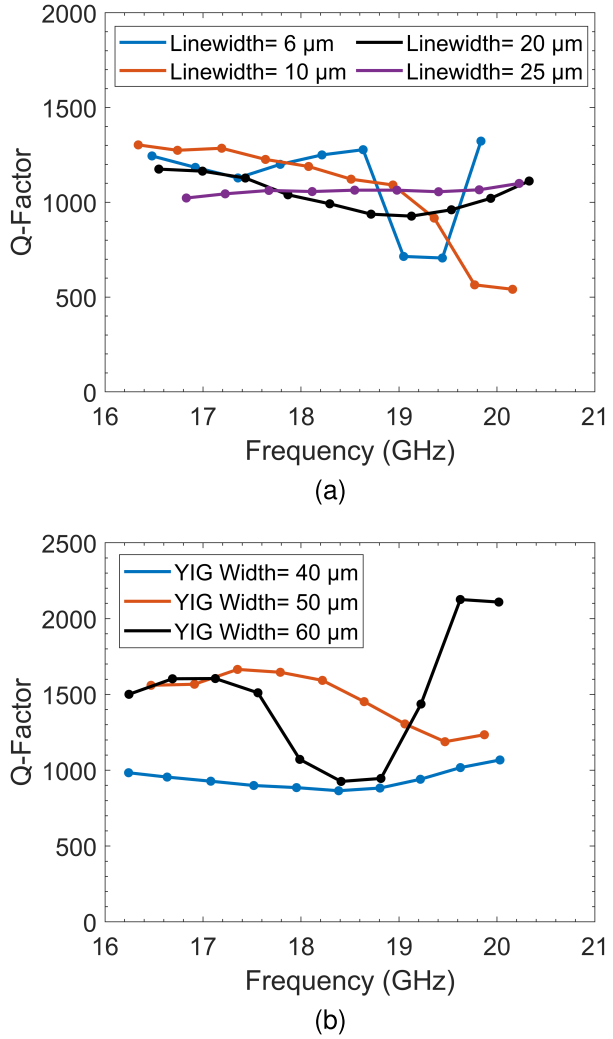

Fig. 10. Measured Q-factor over resonant frequency. (a) YIG resonator width is fixed to 40 μm and the linewidth of the gold transducer is varied. (b) Gold transducer width is fixed to 15 μm and the YIG resonator width is varied.

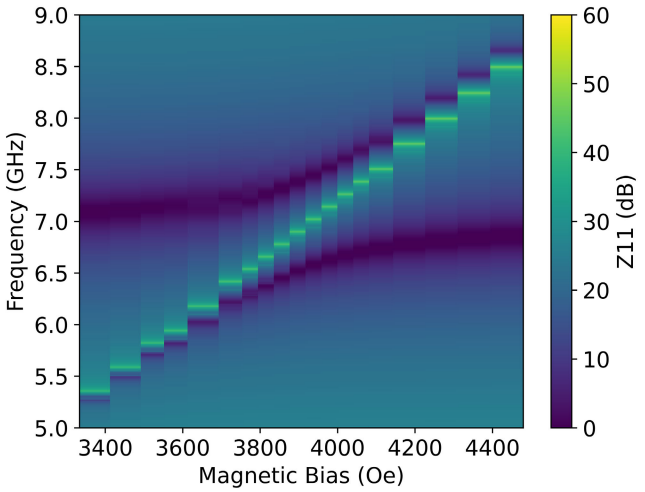

Fig. 11. Measured resonator impedance response at an input RF power of −15 dBm as the applied magnetic field is swept. When the MSW is tuned to overlap with the distributed resonator, the modes interact strongly and an avoided crossing of the anti-resonance is clearly visible.

trend for wider transducer widths up to 20 μm beyond which it decreases. In addition to the radial stub terminated resonators, shorted resonators using the same metal process and similar YIG dimensions were fabricated. Compared with the radial stub resonator [Fig. 7(b)] with a coupling of 13.30% and Q of 376 at 7 GHz, the shorted resonator showed a coupling of 3.03% and Q of 362 at the same frequency, thus experimentally confirming the coupling enhancement without Q-factor degradation.

V. Conclusion

We report a novel MSW resonator coupled to a distributed electromagnetic resonator using state-of-the-art micromachining fabrication techniques. The magnetostatic coupling boost can be precisely controlled through the design of a radial stub termination and we demonstrate both 7- and 18-GHz resonators for C-band and Ku-band operation, respectively. The resonator figure of merit ($k^2_{\text{eff}} \cdot Q$) peaks at 50 for the 7-GHz and at 121 for the 18-GHz surpassing state-of-the-art piezoelectric resonators at similar frequencies [7], [8], [9], [49], [50]. Since k^2_{eff} varies over frequency, a filter design using these resonators must make a tradeoff between maximum bandwidth and center frequency tuning range. Both the insertion loss and ripple increase as either the center frequency is tuned away from the maximum k^2_{eff} or the bandwidth is increased. Interestingly, as the magnetic resonance is tuned to coincide with the distributed electromagnetic resonance, a clear avoided crossing of the anti-resonance is observed in Fig. 11. The response is indicative of a hybridized mode where the magnetostatic wave (magnon) is coupled to the electromagnetic wave (photon). If the one-port resonator is instead coupled to a two-port transmission structure, then the avoided crossing in the transmission spectrum of S21 would be visible. Substituting the gold transducers with a superconductor such as Nb or NbN and cooling the device to cryogenic temperatures opens up applications in magnon–photon hybrid quantum systems [51], [52], [53], [54], [55], [56]. The lithographically defined devices allow flexible integration of the long-lifetime spin waves in YIG with superconducting quantum platforms for novel quantum information processing, sensing, and networking opportunities.

Appendix

The resonator Smith plot in Fig. 12 shows a higher order spurious MSFVW width mode at the small loop near the normalized impedance, $Z = 0.5 + j1$. An ideal resonator should perfectly trace out the circumference of the Smith chart (indicating a purely reactive response without loss) and be free of similar loops and notches indicating spurious resonances. The response of an MSFVW resonator cannot be free of spurious modes, but they can be further suppressed through resonator geometry optimization. The anti-resonance impedance (left side of the Smith plot) can be improved by minimizing the resistance of the transducer. Significantly improving the MSFVW resonance impedance (right side of the Smith plot) is more challenging and requires an investigation into the loss mechanisms of spin waves.

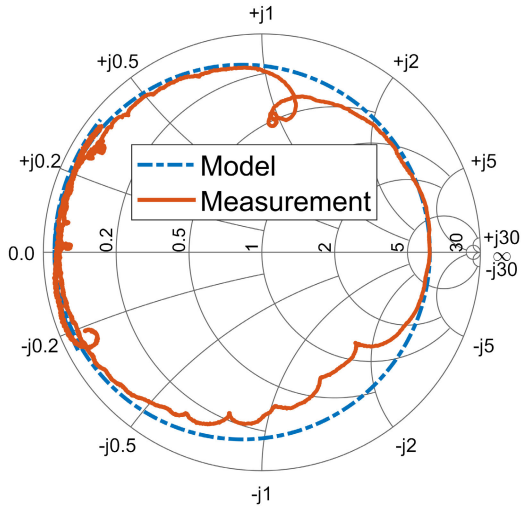

Fig. 12. Smith plot with 50-Ω reference impedance of the measured resonator response (Fig. 6) at 7714 Oe with $f_m = 18.16$ GHz alongside the fit distributed circuit model response.

Data Availability

The code and data used to produce the plots within this work will be provided upon reasonable request.

Acknowledgment

Chip fabrication was performed at the Birck Nanotechnology Center at Purdue University. Resonator characterization, and measurements were performed at Seng-Liang Wang Hall at Purdue. The views, opinions and/or findings expressed are those of the authors and should not be interpreted as representing the official views or policies of the Department of Defense or U.S. Government. This manuscript is approved for public release; distribution A: distribution unlimited. Connor Devitt and Sudhanshu Tiwari designed the resonators. Renyuan Wang designed the patterned plating process. Chip fabrication, resonator measurement, and filter simulations were performed by Connor Devitt. Manuscript was prepared by Connor Devitt with inputs from Sudhanshu Tiwari, Sunil A. Bhave, and Renyuan Wang.

References

[1] G. Ariturk, N. R. Almuqati, and H. H. Sigmarsson, "Element-level microwave filter integration in fully-digital phased array radar systems," in *Proc. IEEE 22nd Annu. Wireless Microw. Technol. Conf.*, Clearwater, FL, USA, Apr. 2022, pp. 1–4. [Online]. Available: https://ieeexplore.ieee.org/document/9786104/

[2] C. Drubin, "Filtering out interference for next-generation wideband arrays," *Microw. J.*, vol. 64, no. 8, pp. 35–36, 2021.

[3] S. H. Talisa, K. W. O'Haver, T. M. Comberiate, M. D. Sharp, and O. F. Somerlock, "Benefits of digital phased array radars," *Proc. IEEE*, vol. 104, no. 3, pp. 530–543, Mar. 2016. [Online]. Available: http://ieeexplore.ieee.org/document/7399690/

[4] R. V. Snyder, G. Macchiarella, S. Bastioli, and C. Tomassoni, "Emerging trends in techniques and technology as applied to filter design," *IEEE J. Microw.*, vol. 1, no. 1, pp. 317–344, Jan. 2021. [Online]. Available: https://ieeexplore.ieee.org/document/9318743/

[5] R. Aigner, "SAW and BAW technologies for RF filter applications: A review of the relative strengths and weaknesses," in *Proc. IEEE Ultrason. Symp.*, Beijing, China, Nov. 2008, pp. 582–589. [Online]. Available: http://ieeexplore.ieee.org/document/4803350/

[6] A. Hagelauer et al., "From microwave acoustic filters to millimeter-wave operation and new applications," *IEEE J. Microw.*, vol. 3, no. 1, pp. 484–508, Jan. 2023. [Online]. Available: https://ieeexplore.ieee.org/document/9994579/

[7] Y. Yang, R. Lu, and S. Gong, "Scaling acoustic filters towards 5G," in *IEDM Tech. Dig.*, San Francisco, CA, USA, Dec. 2018, p. 39. [Online]. Available: https://ieeexplore.ieee.org/document/8614699/

[8] O. Barrera et al., "Thin-film lithium niobate acoustic filter at 23.5 GHz with 2.38 dB IL and 18.2% FBW," *J. Microelectromech. Syst.*, vol. 32, no. 6, pp. 622–625, Dec. 2023, doi: 10.1109/JMEMS.2023.3314666.

[9] M. M. A. Fiagbenu et al., "A K-band bulk acoustic wave resonator using periodically poled $Al_{0.72}Sc_{0.28}N$," *IEEE Electron Device Lett.*, vol. 44, no. 7, pp. 1196–1199, Jul. 2023.

[10] Y. Zou et al., "Aluminum scandium nitride thin-film bulk acoustic resonators for 5G wideband applications," *Microsyst. Nanoeng.*, vol. 8, no. 1, p. 124, Nov. 2022, doi: 10.1038/s41378-022-00457-0.

[11] G. Giribaldi, L. Colombo, P. Simeoni, and M. Rinaldi, "Compact and wideband nanoacoustic pass-band filters for future 5G and 6G cellular radios," *Nature Commun.*, vol. 15, no. 1, Jan. 2024, doi: 10.1038/s41467-023-44038-9.

[12] R. Marcelli, P. De Gasperis, and L. Marescialli, "A tunable, high Q magnetostatic volume wave oscillator based on straight edge YIG resonators," *IEEE Trans. Magn.*, vol. 27, no. 6, pp. 5477–5479, Nov. 1991. [Online]. Available: http://ieeexplore.ieee.org/document/278876/

[13] S. A. Manuilov, R. Fors, S. I. Khartsev, and A. M. Grishin, "Submicron $Y_3Fe_5O_{12}$ film magnetostatic wave band pass filters," *J. Appl. Phys.*, vol. 105, no. 3, Feb. 2009, Art. no. 033917. [Online]. Available: https://pubs.aip.org/jap/article/105/3/033917/383718/Submicron-Y3Fe5O12-Film-Magnetostatic-Wave-Band

[14] J. Adam, "An MSW tunable bandpass filter," in *Proc. IEEE Ultrason. Symp.*, San Francisco, CA, USA, Mar. 1985, pp. 157–162. [Online]. Available: http://ieeexplore.ieee.org/document/1535436/

[15] S. M. Hanna and S. Zeroug, "Single and coupled MSW resonators for microwave channelizers," *IEEE Trans. Magn.*, vol. 24, no. 6, pp. 2808–2810, Nov. 1988. [Online]. Available: http://ieeexplore.ieee.org/document/92252/

[16] G.-M. Yang, J. Wu, J. Lou, M. Liu, and N. X. Sun, "Low-loss magnetically tunable bandpass filters with YIG films," *IEEE Trans. Magn.*, vol. 49, no. 9, pp. 5063–5068, Sep. 2013. [Online]. Available: http://ieeexplore.ieee.org/document/6508942/

[17] Y. Zhang et al., "Nonreciprocal isolating bandpass filter with enhanced isolation using metallized ferrite," *IEEE Trans. Microw. Theory Techn.*, vol. 68, no. 12, pp. 5307–5316, Dec. 2020. [Online]. Available: https://ieeexplore.ieee.org/document/9238458/

[18] *YIG Filters*. Accessed: May 10, 2023. [Online]. Available: https://www.teledynedefenseelectronics.com/wireless/YIG%20Products/Pages/YIG%20Filters.aspx

[19] P. C. Fletcher and R. O. Bell, "Ferrimagnetic resonance modes in spheres," *J. Appl. Phys.*, vol. 30, no. 5, pp. 687–698, May 1959. [Online]. Available: https://pubs.aip.org/jap/article/30/5/687/162486/Ferrimagnetic-Resonance-Modes-in-Spheres

[20] P. S. Carter, "Magnetically-tunable microwave filters using single-crystal yttrium-iron-garnet resonators," *IEEE Trans. Microw. Theory Techn.*, vol. MTT-9, no. 3, pp. 252–260, May 1961. [Online]. Available: http://ieeexplore.ieee.org/document/1125316/

[21] W. S. Ishak, "Magnetostatic wave technology: A review," *Proc. IEEE*, vol. 76, no. 2, pp. 171–187, Feb. 1988. [Online]. Available: http://ieeexplore.ieee.org/document/4393/

[22] W. S. Ishak and K.-W. Chang, "Tunable microwave resonators using magnetostatic wave in YIG films," *IEEE Trans. Microw. Theory Techn.*, vol. MTT-34, no. 12, pp. 1383–1393, Dec. 1986. [Online]. Available: http://ieeexplore.ieee.org/document/1133553/

[23] X. Du et al., "Frequency tunable magnetostatic wave filters with zero static power magnetic biasing circuitry," 2023, *arXiv:2308.00907*.

[24] V. V. Tikhonov, A. N. Litvinenko, S. A. Nikitov, and S. G. Suchkov, "Temperature stabilization of spin-wave ferrite devices," *J. Commun. Technol. Electron.*, vol. 58, no. 1, pp. 75–81, Jan. 2013, doi: 10.1134/S1064226913010075.

[25] C. Devitt, R. Wang, S. Tiwari, and S. A. Bhave, "An edge-coupled magnetostatic bandpass filter," 2023, *arXiv:2312.10583*.

[26] S. Dai, S. A. Bhave, and R. Wang, "Octave-tunable magnetostatic wave YIG resonators on a chip," *IEEE Trans. Ultrason., Ferroelectr., Freq. Control*, vol. 67, no. 11, pp. 2454–2460, Nov. 2020. [Online]. Available: https://ieeexplore.ieee.org/document/9108306/

[27] R. Marcelli, G. Sajin, and A. Cismaru, "Band-pass magnetostatic wave resonators on micromachined silicon substrate," *Rev. Sci. Instrum.*, vol. 75, no. 4, pp. 1127–1133, Apr. 2004. [Online]. Available: https://pubs.aip.org/rsi/article/75/4/1127/466503/Band-pass-magnetostatic-wave-resonators-on

[28] J. D. Costa et al., "Compact tunable YIG-based RF resonators," *Appl. Phys. Lett.*, vol. 118, no. 16, Apr. 2021, Art. no. 162406. [Online]. Available: https://pubs.aip.org/apl/article/118/16/162406/1062227/Compact-tunable-YIG-based-RF-resonators

[29] D. A. Connelly, "Principles, modeling, and measurement towards efficient microwave spin-wave circuits," Ph.D. dissertation, Dept. Elect. Eng., Univ. Notre Dame, Notre Dame, Indiana, 2023.

[30] Y. Feng, S. Tiwari, S. A. Bhave, and R. Wang, "Micromachined tunable magnetostatic forward volume wave bandstop filter," *IEEE Microw. Wireless Technol. Lett.*, vol. 33, no. 6, pp. 807–810, Jun. 2023. [Online]. Available: https://ieeexplore.ieee.org/document/10111074/

[31] Q. Gao, M. E. Fordham, W. Gu, H. Cui, and Y. E. Wang, "Design RF magnetic devices with linear and nonlinear equivalent circuit models: Demystify RF magnetics with equivalent circuit models," *IEEE Microw. Mag.*, vol. 23, no. 11, pp. 28–47, Nov. 2022. [Online]. Available: https://ieeexplore.ieee.org/document/9910195/

[32] Q. Gao, "An equivalent circuit model for tunable bandpass filters based on ferromagnetic resonance," M.S. thesis, Dept. Elect. Comput. Eng. UCLA, Univ. California, Los Angeles, CA, USA, 2021. [Online]. Available: https://www.proquest.com/dissertations-theses/equivalent-circuit-model-tunable-bandpass-filters/docview/2555310965/se-2?accountid=13360

[33] H. Cui, Z. Yao, and Y. E. Wang, "Coupling electromagnetic waves to spin waves: A physics-based nonlinear circuit model for frequency-selective limiters," *IEEE Trans. Microw. Theory Techn.*, vol. 67, no. 8, pp. 3221–3229, Aug. 2019. [Online]. Available: https://ieeexplore.ieee.org/document/8736517/

[34] D. D. Stancil, *Theory of Magnetostatic Waves*. New York, NY, USA: Springer, 1993, doi: 10.1007/978-1-4613-9338-2.

[35] W. S. Ishak, C. Kok-Wai, W. E. Kunz, and G. Miccoli, "Tunable microwave resonators and oscillators using magnetostatic waves," *IEEE Trans. Ultrason., Ferroelectr., Freq. Control*, vol. 35, no. 3, pp. 396–405, May 1988. [Online]. Available: http://ieeexplore.ieee.org/document/20461/

[36] K.-Y. Hashimoto and S. M. Wrobel, *RF Bulk Acoustic Wave Filters for Communications*. Norwood, MA, USA: Artech House, 2009. [Online]. Available: http://ebookcentral.proquest.com/lib/purdue/detail.action?docID=456907

[37] J. D. Larson, P. D. Bradley, S. Wartenberg, and R. C. Ruby, "Modified Butterworth-Van Dyke circuit for FBAR resonators and automated measurement system," in *Proc. IEEE Ultrason. Int. Symp.*, San Juan, PR, USA, Oct. 2000, pp. 863–868. [Online]. Available: https://ieeexplore.ieee.org/document/922679/

[38] D. Psychogiou, R. Gómez-García, R. Loeches-Sánchez, and D. Peroulis, "Hybrid acoustic-wave-lumped-element resonators (AWLRs) for high-Q bandpass filters with quasi-elliptic frequency response," *IEEE Trans. Microw. Theory Techn.*, vol. 63, no. 7, pp. 2233–2244, Jul. 2015. [Online]. Available: http://ieeexplore.ieee.org/document/7122936/

[39] Y. Yang, L. Gao, and S. Gong, "X-band miniature filters using lithium niobate acoustic resonators and bandwidth widening technique," *IEEE Trans. Microw. Theory Techn.*, vol. 69, no. 3, pp. 1602–1610, Mar. 2021. [Online]. Available: https://ieeexplore.ieee.org/document/9337207/

[40] P. A. Truitt, J. B. Hertzberg, C. C. Huang, K. L. Ekinci, and K. C. Schwab, "Efficient and sensitive capacitive readout of nanomechanical resonator arrays," *Nano Lett.*, vol. 7, no. 1, pp. 120–126, Jan. 2007, doi: 10.1021/nl062278g.

[41] B. Cagdaser and B. E. Boser, "Low-voltage electrostatic actuation with inherent position feedback," *J. Microelectromech. Syst.*, vol. 21, no. 5, pp. 1187–1196, Oct. 2012. [Online]. Available: http://ieeexplore.ieee.org/document/6199945/

[42] S. Barzanjeh et al., "Mechanical on-chip microwave circulator," *Nature Commun.*, vol. 8, no. 1, p. 953, Oct. 2017. [Online]. Available: https://www.nature.com/articles/s41467-017-01304-x

[43] Q. Yang, W. Pang, D. Zhang, and H. Zhang, "A modified lattice configuration design for compact wideband bulk acoustic wave filter applications," *Micromachines*, vol. 7, no. 8, p. 133, Aug. 2016. [Online]. Available: http://www.mdpi.com/2072-666X/7/8/133

[44] J. Xie, M. Shen, Y. Xu, W. Fu, L. Yang, and H. X. Tang, "Sub-terahertz electromechanics," *Nature Electron.*, vol. 6, no. 4, pp. 301–306, Mar. 2023. [Online]. Available: https://www.nature.com/articles/s41928-023-00942-y

[45] B. C. Wadell, *Transmission Line Design Handbook* (The Artech House Microwave Library). Boston, MA, USA: Artech House, 1991.

[46] H. Asao, H. Oh-Hashi, T. Ohwada, and O. I. Members, "A tunable oscillator using magnetostatic forward-volume wave resonator with wide strip transducer," *Electron. Commun. Jpn.*, vol. 78, no. 5, pp. 81–91, May 1995.

[47] S. Zhang, X. Meng, X. Zheng, S. R. Das, and F. Shepherd, "Process for uniformly electroplating a patterned wafer with electrically isolated devices," *J. Vac. Sci. Technol. A, Vac., Surf., Films*, vol. 22, no. 3, pp. 1079–1082, May 2004. [Online]. Available: https://pubs.aip.org/jva/article/22/3/1079/1072216/Process-for-uniformly-electroplating-a-patterned

[48] J. S. Pulskamp et al., "Monolithically integrated PiezoMEMS SP2T switch and contour-mode filters," in *Proc. IEEE 22nd Int. Conf. Micro Electro Mech. Syst.*, Sorrento, Italy, Jan. 2009, pp. 900–903. [Online]. Available: http://ieeexplore.ieee.org/document/4805529/

[49] G. Giribaldi, L. Colombo, and M. Rinaldi, "6–20 GHz 30% ScAlN lateral field-excited cross-sectional Lamé mode resonators for future mobile RF front ends," *IEEE Trans. Ultrason., Ferroelectr., Freq. Control*, vol. 70, no. 10, pp. 1201–1212, Oct. 2023. [Online]. Available: https://ieeexplore.ieee.org/document/10243055/

[50] J. Kramer et al., "Thin-film lithium niobate acoustic resonator with high Q of 237 and k^2 of 5.1% at 50.74 GHz," in *Proc. Joint Conf. Eur. Frequency Time Forum IEEE Int. Frequency Control Symp.*, Toyama, Japan, May 2023, pp. 1–4. [Online]. Available: https://ieeexplore.ieee.org/document/10272149/

[51] L. McKenzie-Sell, J. Xie, C.-M. Lee, J. W. A. Robinson, C. Ciccarelli, and J. A. Haigh, "Low-impedance superconducting microwave resonators for strong coupling to small magnetic mode volumes," *Phys. Rev. B, Condens. Matter*, vol. 99, no. 14, Apr. 2019, Art. no. 140414, doi: 10.1103/PhysRevB.99.140414.

[52] S. Guo, D. Russell, J. Lanier, H. Da, P. C. Hammel, and F. Yang, "Strong on-chip microwave photon–magnon coupling using ultralow-damping epitaxial $Y_3Fe_5O_{12}$ films at 2 K," *Nano Lett.*, vol. 23, no. 11, pp. 5055–5060, Jun. 2023, doi: 10.1021/acs.nanolett.3c00959.

[53] J. Xu et al., "Cryogenic hybrid magnonic circuits based on spalled YIG thin films," 2023, *arXiv:2312.10660*.

[54] Q. Xu et al., "Strong photon-magnon coupling using a lithographically defined organic ferrimagnet," *Adv. Sci.*, vol. 11, no. 14, 2024, Art. no. 2310032, doi: 10.1002/advs.202310032.

[55] P. G. Baity et al., "Strong magnon–photon coupling with chip-integrated YIG in the zero-temperature limit," *Appl. Phys. Lett.*, vol. 119, no. 3, Jul. 2021, Art. no. 033502. [Online]. Available: https://pubs.aip.org/apl/article/119/3/033502/41793/Strong-magnon-photon-coupling-with-chip-integrated

[56] J. Xu, C. Zhong, X. Han, D. Jin, L. Jiang, and X. Zhang, "Dynamical control in hybrid magnonics," *Proc. SPIE*, vol. 12656, pp. 116–121, Sep. 2023. [Online]. Available: https://www.spiedigitallibrary.10.1021/nl062278gorg/conference-proceedings-of-spie/12656/2677206/Dynamical-control-in-hybrid-magnonics/10.1117/12.2677206.full